

Article

Surface Modification of Fe-ZSM-5 Using Mg for a Reduced Catalytic Pyrolysis Temperature of Low-Density Polyethylene to Produce Light Olefin

Yincui Li, Ting Liu, Shengnan Deng, Xiao Liu, Qian Meng, Mengxue Tang, Xueying Wu and Huawei Zhang *

School of Environmental and Municipal Engineering, Qingdao University of Technology, Qingdao 266033, China; liyincui9bumy@163.com (Y.L.); liuting@qut.edu.cn (T.L.); dengshengnan1998@163.com (S.D.); liuxiao202306@163.com (X.L.); m15253879062@163.com (Q.M.); tangerine1108@163.com (M.T.); wuxueying0225@163.com (X.W.)

* Correspondence: zhanghuawei@qut.edu.cn

Abstract: Although the catalytic pyrolysis of low-density polyethylene (LDPE) to produce light olefin has shown potential industrial application advantages, it has generally suffered when using higher pyrolysis temperatures. In this work, Mg-modified Fe-ZSM-5 was used for catalytic conversion of LDPE to obtain light olefin in a fixed bed reactor. The effects of catalyst types, pyrolysis temperatures, and Mg loading on the yield of light olefin were investigated. The 1 wt% Mg loading slightly improved the yield of light olefin to 38.87 wt% at 395 °C, lowering the temperature of the pyrolysis reaction. We considered that the higher light olefin yield of Fe-Mg-ZSM-5 was attributed to the introduction of Mg, where Mg regulated the surface acidity of the catalyst, inhibited the secondary cracking reaction, and reduced coking during the pyrolysis process. Furthermore, the addition of Mg also dramatically reduced the average particle size of Fe oxides from 40 nm to 10 nm, which is conducive to a lower catalytic reaction temperature. Finally, the spent catalyst could be easily regenerated at the conditions of 600 °C in airflow with a heating rate of 10 °C/min for 1 h, and the light olefin yield remained higher than 36.71 wt% after five cycles, indicating its excellent regeneration performance.

Keywords: catalytic pyrolysis; LDPE; Fe-Mg-ZSM-5; light olefin; pyrolysis temperature



Citation: Li, Y.; Liu, T.; Deng, S.; Liu, X.; Meng, Q.; Tang, M.; Wu, X.; Zhang, H. Surface Modification of Fe-ZSM-5 Using Mg for a Reduced Catalytic Pyrolysis Temperature of Low-Density Polyethylene to Produce Light Olefin. *Catalysts* **2024**, *14*, 78. <https://doi.org/10.3390/catal14010078>

Academic Editor: Tomás García

Received: 9 December 2023

Revised: 29 December 2023

Accepted: 12 January 2024

Published: 18 January 2024



Copyright: © 2024 by the authors. Licensee MDPI, Basel, Switzerland. This article is an open access article distributed under the terms and conditions of the Creative Commons Attribution (CC BY) license (<https://creativecommons.org/licenses/by/4.0/>).

1. Introduction

Nowadays, waste plastics are being generated at an increasing rate, which has caused serious problems for both the environment and human health [1,2]. Notably, waste plastics have an EHI value of up to 2 [3] and can be applied as a source of high-quality fuel during the pyrolysis process. Low-density polyethylene (LDPE) is one of the most extensively used plastics [3], accounting for 38% of the total plastic produced [4]. It has a high degree of short- and long-chain branching [5] and a very high carbon and hydrogen content due to the polymer's structure [6], making it an excellent raw resource. Therefore, the conversion of LDPE into high-value-added products is an essential challenge from both an environmental and an industrial point of view [7].

Pyrolysis is an effective process for the resource utilization of LDPE [8]. Traditional pyrolysis products are composed of three phases including gas, liquid, and solid, in which the gas product is mainly hydrocarbon species, the solid product is coke, and the liquid product is a mixture of wax and oil [9]. In the pyrolysis process, LDPE mainly follows the linear random chain breaking mechanism and chain end breaking mechanism [10], forming different lengths of primary free radical fragments, and a small number of primary free radical fragments are further formed as olefins through β breaking [11]. Light olefin (consisting of ethylene, propylene, and butylene) is an essential component of petrochemical industries, which can be used in the production of polyethylene, butadiene, and other

chemical feedstocks [12]. The demand for light olefin has increased in recent decades [13]. Therefore, using LDPE as a feedstock provides a unique approach to producing light olefin, which is necessary to expand the market and meet the demand for light olefin [12].

However, the pyrolysis of LDPE generally suffers from high reaction temperatures and unregulated pyrolysis products [5,14]. In order to obtain a high yield of chemical raw materials, the pyrolysis temperature will sometimes be as high as 700–900 °C [15,16]. Hasret Akgün et al. [6] conducted pyrolysis experiments on LDPE at different temperatures; the results showed that LDPE had the highest liquid-phase yield (85.87%) at 800 °C with a heating rate of 5 °C/min, and the liquid-phase product was heavy wax. Maite Artetxe et al. [17] found that continuously feeding plastic into a conical spray bed reactor (CSBR) operating at 500 °C produced 93% wax (C_{21}^+) and C_{12} – C_{21} hydrocarbons. It has been reported that the presence of catalysts not only greatly enhances the quality and quantity of the desired products by improving the conversion efficiency, but also dramatically decreases pyrolysis temperatures [18]. The catalytic pyrolysis of LDPE mainly follows the carbocation reaction mechanism [10]. A variety of catalysts such as ZSM-5, zeolite, Y-zeolite, FCC, and MCM-41 have been widely used in the catalytic pyrolysis process of LDPE [19,20].

ZSM-5 zeolite is a popular material for light olefin production due to its three-dimensional regular pore structure, good hydrothermal stability, and selective shape catalysis [21]. It is often modified by transition metals such as Fe, Ga, Ni, and La to regulate acid strength, which is beneficial for the enhancement of light olefin selectivity [22]. Li et al. [23] tested the catalytic cracking of bio-oil model compounds on La_2O_3 -modified ZSM-5 zeolites to generate light olefin; the obtained light olefin consisted of C_3H_6 (13.6–17.1%), C_2H_4 (10.7–15.4%), and C_4H_8 (5.3–6.3%). Lima et al. [24] evaluated the catalytic performance of glycerol pyrolysis to produce light olefin on Fe-, Mo-, and Nb-loaded HZSM-5; they found that Fe-ZSM-5 has a maximum selectivity of propylene at lower temperatures because of its strong acidity. Wang et al. [22] reported that an Fe@NS catalyst achieved 41.8 wt% yields of light olefin at a pyrolysis temperature of 550 °C and a weight hourly space velocity of 8.64 h^{-1} . Xia et al. [25] found that the highest light olefin yield of 44.8 wt% was obtained from an Al-Fe-SPZ catalyst for cracking n-heptane when the Si/(Al + Fe) molar ratio was 100 and the Al/Fe ratio was 84/16. Zhang et al. [12] studied the conversion of biomass into light olefin over Fe-loaded ZSM-5 catalysts; they revealed that 6.98% of light olefin was achieved on 3 wt% Fe-ZSM-5 at a temperature of 600 °C. Shao et al. [26] investigated the rapid pyrolysis of cellulose catalyzed by Fe-, La-, Cu-, Mg-, Al-, and Ce-modified ZSM-5 zeolite to obtain light olefin, and the results suggested that Cu-ZSM-5 had the maximum yield of light olefin. Although a considerable number of catalysts have been studied, the catalytic pyrolysis of LDPE still has the challenges of high reaction temperatures and a low yield of light olefin. Therefore, it is necessary to develop more efficient and renewable catalysts.

In this study, we prepared an Fe-Mg-ZSM-5 catalyst and performed catalytic pyrolysis of LDPE in a fixed-bed reactor for the selective generation of light olefin. Our main aim is to identify the increasing yield of light olefin as well as the decreasing reaction temperature. Combining contrasted design experiments as well as BET, NH_3 -TPD, XRD, SEM, TEM/EDS, and DTG/TGA characterization, the role of Mg loading was explored, which offered a sufficient and thorough explanation of the transformation of light olefin. In addition, the regeneration performance of deactivated catalysts was also investigated for recyclable, sustainable, and economic utilization.

2. Results and Discussion

2.1. Catalyst Characterization

2.1.1. BET Results

The structural properties of the various catalysts are shown in Table S1. It can be seen that the BET surface areas of ZSM-5 were $329\text{ m}^2\cdot\text{g}^{-1}$, which decreased to $293\text{ m}^2\cdot\text{g}^{-1}$ with the presentation of 1 wt% Fe oxides, and then slightly increased to $308\text{ m}^2\cdot\text{g}^{-1}$ with

the doping of 1 wt% Mg oxides. The decrease in both the surface area and volume of the micropores of ZSM-5 indicated that parts of the Fe and Mg oxides diffused into the pores and or covered the pore channels of ZSM-5, which resulted in the blocking of micropores [27]. At the same time, it was found the average pore size of ZSM-5 increased from 2.89 nm to 3.37 nm and 3.22 nm after the loading of Fe and Fe-Mg oxides, indicating that the metal ions are dispersed throughout the ZSM-5 surface [28,29].

2.1.2. NH₃-TPD Results

The NH₃-TPD fitting results of the different catalysts are depicted in Figure 1. The spectra of catalysts can be fitted by three peaks centered at 140 °C, 210 °C, and 430 °C, which are attributed to the weak, medium, and strong acidity of the samples, respectively [12,24]. Weak acidity is attributed to the weak Brønsted acid and Lewis acid on the surface of ZSM-5, which has been verified to show little catalytic activity for LDPE pyrolysis [27]. Medium acidity corresponds to strong Brønsted acidic sites [30], which have a remarkable effect on the yield of light olefin [27]. Strong acidity is related to strong Lewis acidic sites [28], which is considered the key contributor to the coking of the catalyst during the pyrolysis process [30].

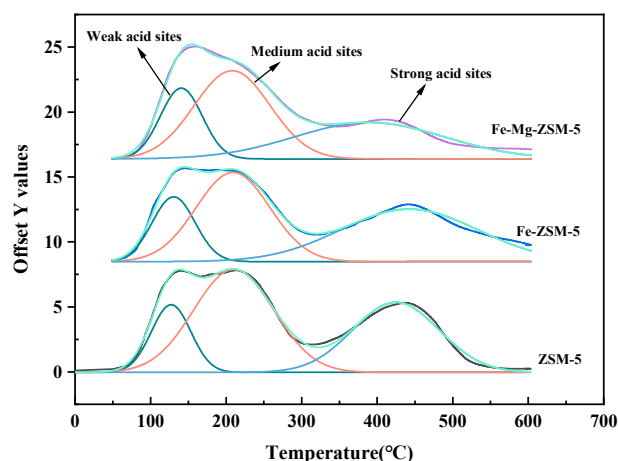


Figure 1. NH₃-TPD curve of the different catalysts.

The fitting results of the acid distribution on the different catalysts are presented in Table 1. The total acid content of the catalyst reduced from 1320 $\mu\text{mol}\cdot\text{g}^{-1}$ to 1089 $\mu\text{mol}\cdot\text{g}^{-1}$ and 1094 $\mu\text{mol}\cdot\text{g}^{-1}$ after Fe and Mg were loaded onto ZSM-5. It can be observed that the introduction of Fe oxides boosted the strong acidity of the ZSM-5 catalyst, which increased from 470.71 $\mu\text{mol}\cdot\text{g}^{-1}$ to 473.72 $\mu\text{mol}\cdot\text{g}^{-1}$, respectively. Meanwhile, the loading of Fe oxides also reduced the weak and medium acidity of ZSM-5, which decreased from 206.71 $\mu\text{mol}\cdot\text{g}^{-1}$ and 642.58 $\mu\text{mol}\cdot\text{g}^{-1}$ to 182.52 $\mu\text{mol}\cdot\text{g}^{-1}$ and 432.77 $\mu\text{mol}\cdot\text{g}^{-1}$, respectively. When the Mg oxides were further loaded onto Fe-ZSM-5, it was evident that the strong acidity decreased to 394.93 $\mu\text{mol}\cdot\text{g}^{-1}$, while the weak and medium acidity increased slightly to 214.75 $\mu\text{mol}\cdot\text{g}^{-1}$ and 484.31 $\mu\text{mol}\cdot\text{g}^{-1}$, respectively. This is mainly due to the modification of Mg as an alkali metal covering the strong acid sites on the surface of ZSM-5, causing a significant decline in the number of strong acidities [31].

Table 1. Acidity distribution of the catalysts.

Catalysts	Acid Content ($\mu\text{mol/g}$)			
	Weak Acidity	Medium Acidity	Strong Acidity	Total Acidity
ZSM-5	206.71	642.58	470.71	1320
Fe-ZSM-5	182.52	432.77	473.72	1089
Fe-Mg-ZSM-5	214.75	484.31	394.93	1094

2.1.3. SEM and TEM Results

The SEM and TEM images of ZSM-5, Fe-ZSM-5, and Fe-Mg-ZSM-5 are displayed in Figure 2. It can be seen from the SEM images of the samples in Figure 2a–c that the crystal structure of ZSM-5 zeolite is very regular with a particle size ranging from 250 to 450 nm (Figure 2a), which is composed of clear quadrangular prismatic crystallites [32–34]. After the loading of Fe and Mg oxides, the morphology of the catalyst remained unchanged (Figure 2b,c), illustrating that the modification process did not destroy the crystal structure of ZSM-5. The HRTEM images of the ZSM-5, Fe-ZSM-5, and Fe-Mg-ZSM-5 catalysts in Figure 2d–f prove the successful loading of Fe and Mg oxides onto ZSM-5. As seen in Figure 2e, the Fe oxide particles agglomerated on the surface of ZSM-5, and the particle size ranged from 20 nm to 80 nm with an average particle size of 40 nm. It can be observed in Figure 2f that the Mg loading significantly decreased the particle size of the Fe oxides, which ranged from 5 nm to 25 nm with an average particle size of 10 nm. The Fe and Mg oxides were highly and uniformly dispersed on the ZSM-5 surface without a clustering phenomenon. The high dispersion as well as small particles caused by the Mg loading are conducive to the catalytic activity in the LDPE pyrolysis reaction. Figure 2g shows the corresponding STEM-XEDS element diagram, indicating that the Fe and Mg elements are evenly distributed in the samples.

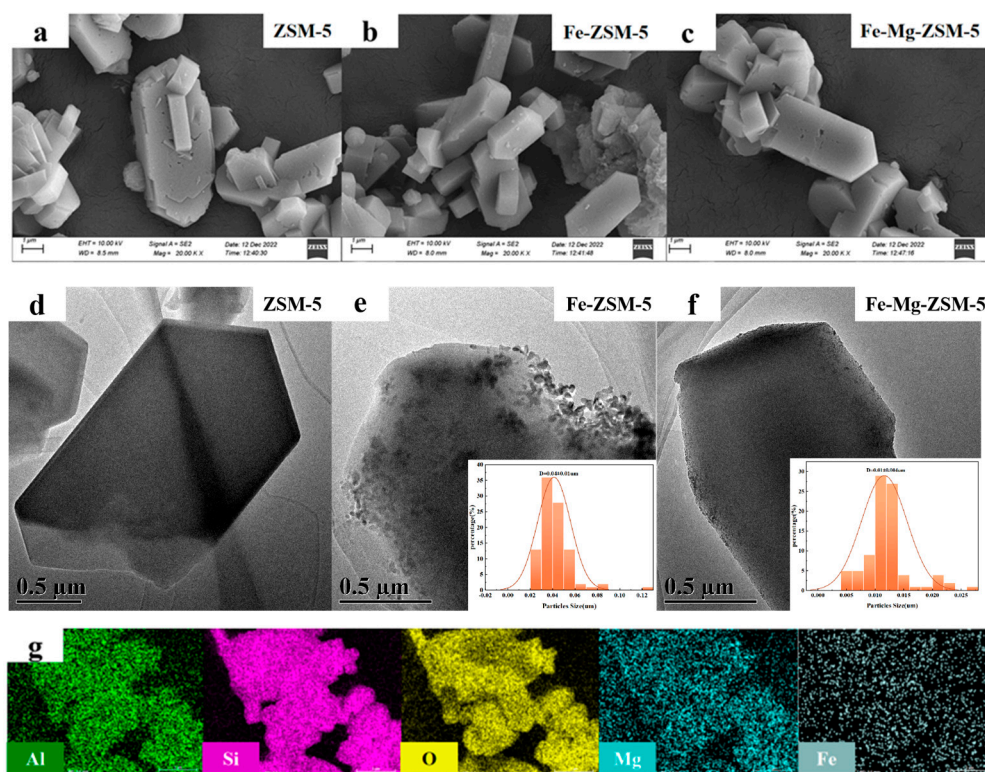


Figure 2. SEM and TEM images of different catalysts. ((a–c) SEM; (d–f) TEM; (g) compositional mapping of Fe-Mg-ZSM-5).

2.1.4. XRD Analysis

The obtained XRD patterns of the ZSM-5, Fe-ZSM-5, and Fe-Mg-ZSM-5 samples are presented in Figure 3. It is clear that the characteristic diffraction peaks at 7.9, 8.8, 9.0, 13.8, 14.7, 15.4, 15.8, 23.0, 23.2, 23.6, 23.9, 24.3, and 29.9° can be observed in three samples [27,35,36]. There is no significant diffraction peak of Fe and Mg oxides in the spectra of the Fe-ZSM-5 and Fe-Mg-ZSM-5 samples, implying the nanoparticles of the Fe and Mg oxides are highly dispersed on the surface of ZSM-5, or the loaded content of metal oxides is too low to be detected with XRD [27,30,37]. The crystallinity of the different catalysts is shown in the Supplementary Materials (Table S2).

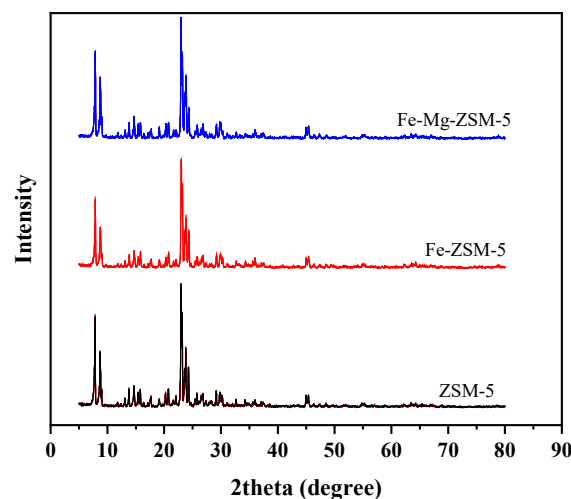


Figure 3. XRD pattern of the catalysts.

2.1.5. XPS Analysis

The XPS spectra of ZSM-5, Fe-ZSM-5, and Fe-Mg-ZSM-5 are exhibited in Figure 4. The full spectra of the three samples in Figure 4a show the peaks of Fe2p and Mg1s that appeared after the modification process, indicating the successful loading of Fe and Mg oxides. As shown in Figure 4b, the Fe2p narrow spectrum of Fe-Mg-ZSM-5 can be fitted with eight peaks: the two peaks at 724.4 eV and 726.1 eV corresponded to the characteristic peaks of Fe2p_{3/2}, and the peaks at 710.8 eV and 712.6 eV correspond to the characteristic peak of Fe at 2p_{1/2}, respectively [38,39]. The four peaks centered at 710.8 eV, 724.4 eV, and 712.6 eV, 726.1 eV were assigned to the satellite peaks of Fe²⁺ and Fe³⁺, indicating the coexistence of FeO and Fe₂O₃ nanoparticles [40]. The Mg1s spectrum in Figure 4c showed a peak at 1304.7 eV, which proved the presence of MgO [41].

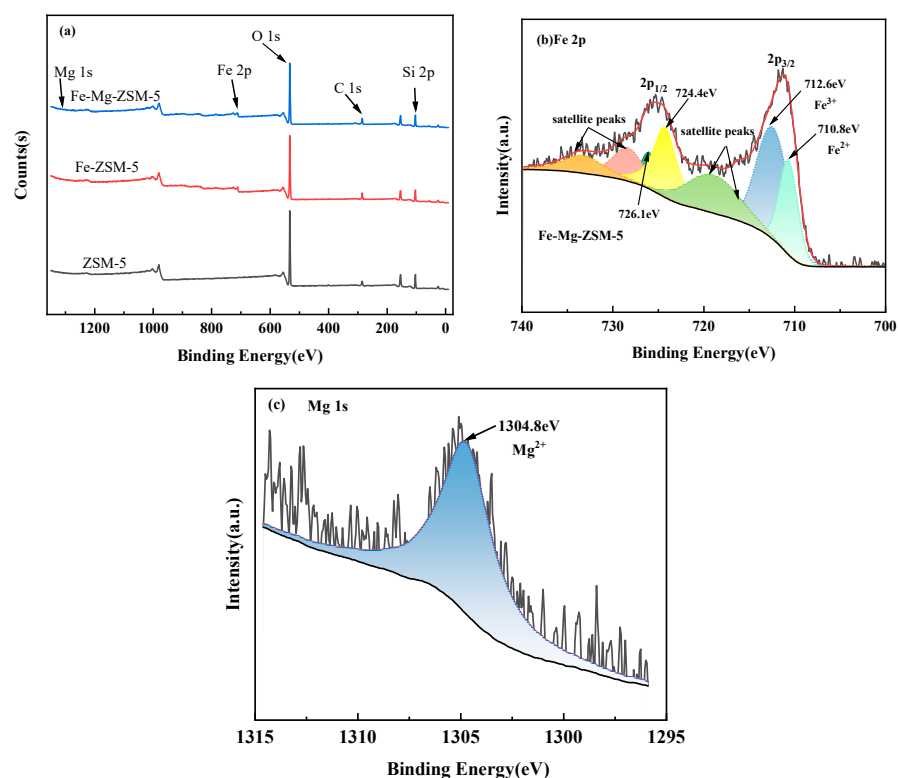


Figure 4. (a) XPS survey scan spectrum of different catalysts; (b) Fe 2p of Fe-Mg-ZSM-5 and (c) Mg 1s of Fe-Mg-ZSM-5.

2.2. The Catalytic Pyrolysis of LDPE on Different Catalysts

2.2.1. Catalysis Performance Comparison of Different Catalysts

In this paper, we explored the effect of the pyrolysis of ZSM-5, Fe-ZSM-5, and Fe-Mg-ZSM-5 with LDPE on light olefin yield. The temperatures at the optimal light olefin yield conditions for different catalysts are shown in Figure 5. According to the results, ZSM-5 reached the highest light olefin yield (32.38 wt%) at 500 °C. It can be seen that the loading of Fe increased the yield of light olefin by 6.08 wt%. At the same time, it reduced the pyrolysis reaction temperature by 75 °C, which was attributed to the uniform distribution and excellent dispersion of Fe oxides on ZSM-5, while the presence of Fe modified the catalyst and improved its activity [42].

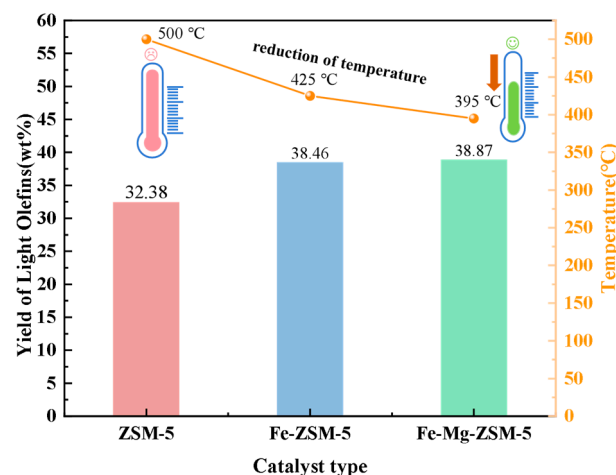


Figure 5. Comparison of optimal light olefin yields with different catalysts.

When the Mg addition was further added to Fe-ZSM-5, the results revealed that while the enhancement in the yield of light olefins was only 0.41 wt%, the temperature was reduced from 425 °C to 395 °C. According to the TEM results (Figure 2), it was found that the introduction of Mg significantly reduced the average particle size of Fe oxides on the catalyst from 40 nm to 10 nm, which was beneficial to improving the catalytic activity and thus decreased the pyrolysis reaction temperature. In addition, the introduction of Mg facilitates the dispersion of Fe oxides [43,44], as well as improves the stability and activity of the Fe-Mg-ZSM-5 catalyst for the catalytic reaction [45].

In addition, Figure 6 further summarizes and compares different conditions for the preparation of light olefins with PE [46–48]. The results showed that although the Fe-Mg-ZSM-5 catalyst did not improve the yield of light olefins significantly, it reduced the pyrolysis temperature and realized the preparation of light olefins at a relatively mild temperature, which saved the energy consumption to a certain extent. The catalytic performance of the three catalysts is described in detail in Section 2.2.2 through Section 2.2.4.

2.2.2. Catalytic Performance of ZSM-5

The results of the LDPE catalytic pyrolysis on ZSM-5 are shown in Figure 7. It can be seen in Figure 7a that the gas yield increased from 74.21% to 85.08% as the temperature increased from 450 °C to 600 °C, while the liquid yield decreased dramatically from 25.17% to 13.32%. This was due to the further cracking of oligomers caused by the further increased temperatures, forming smaller hydrocarbons in the presence of gaseous compounds and reducing the liquid yield [49]. Figure 7b shows that the gas products of LDPE catalytic pyrolysis primarily consisted of H₂, CH₄, C₂–C₄ olefins, and C₂–C₅ alkanes, and light olefins accounted for 35.24% of total gas product at 600 °C. As exhibited in Figure 7c, the production of light olefin increased from 29.94 wt% to 32.38 wt% when the temperature increased from 450 °C to 500 °C and then decreased to 30.02 wt% when the temperature further rose to 600 °C, implying the desired reaction temperature for the target product

is 500 °C. Figure 7d shows that the component of light olefin was also extremely influenced by the pyrolysis temperature. With an increase in temperature, the selectivity of C_3H_6 increased obviously from 48.26% to 61.51%, while the selectivity of C_4H_8 decreased significantly from 48.57% to 35.24%, respectively. The pyrolysis had a negligible effect on the selectivity of C_2H_4 , which remained stable at about 3.25% from 450 °C to 600 °C. In addition, the selectivity of C_3H_6 and C_4H_8 was much higher than that of C_2H_4 ; this might be attributed to the acid inhibition of the olefin hydrogen transfer reaction of ZSM-5, which improves the selectivity of propylene and butene in LDPE cleavage products [22].

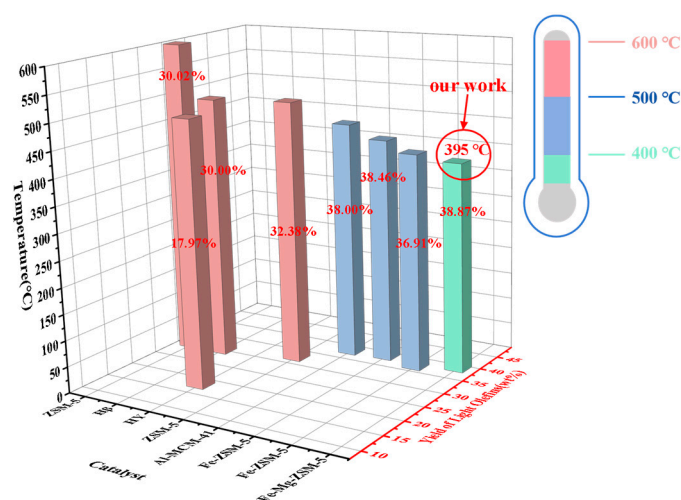


Figure 6. Summary and comparison of light olefin yields under different conditions.

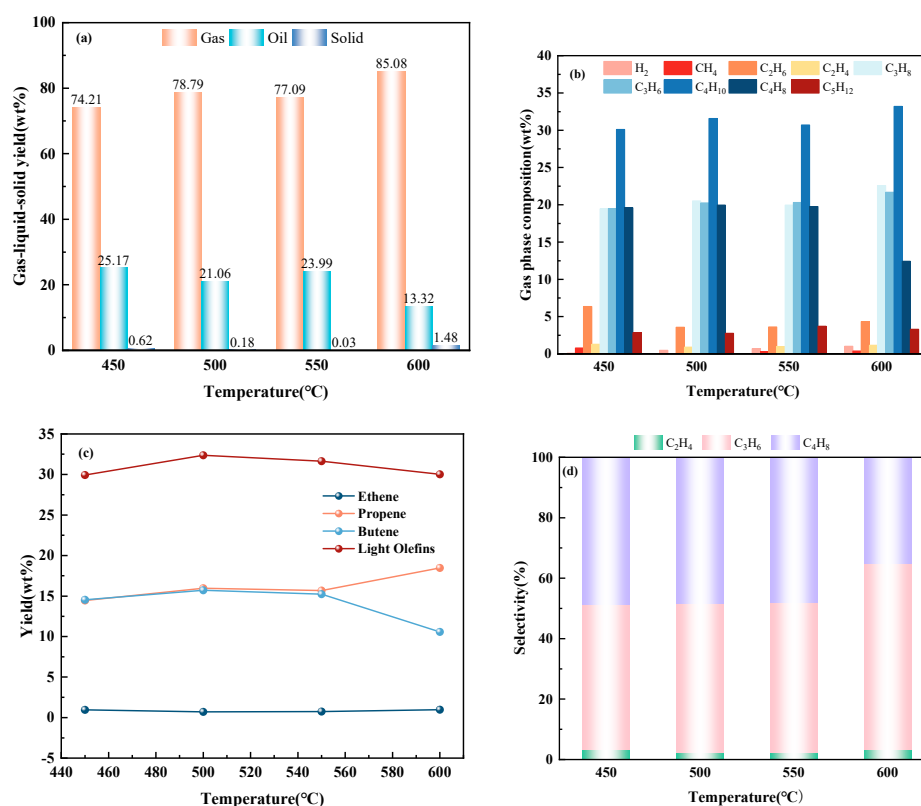


Figure 7. Influence of ZSM-5 on the creation of light olefin: (a) mass percentages of solids, gases, and liquids; (b) percentage by mass of H_2 , CH_4 , light olefin, and C_2 – C_5 alkanes; (c) weight yields of light olefin; and (d) olefin selectivity of C_2H_4 , C_3H_6 , and C_4H_8 .

2.2.3. Catalytic Performance of Fe-ZSM-5

Figure 8 illustrates the influence of Fe loading on the pyrolysis of LDPE on ZSM-5. As seen in Figure 8a, the gas product yield of LDPE catalytic pyrolysis on Fe-ZSM-5 is as high as 88.63 wt% at 425 °C, and the pyrolysis temperature is much lower than that on ZSM-5. The gaseous compounds in Figure 8b are chiefly H₂, CH₄, C₂–C₄ olefins, and C₂–C₅ alkanes, and the light olefins account for 43.39% of total gas product at 425 °C, which is 8.15% higher than that on ZSM-5. Figure 8c shows that the quantity of light olefin increased gradually with the rise in temperatures, where the highest yield of 38.46% was achieved at 425 °C. It is evident that the Fe loading not only reduced the optimal pyrolysis temperature from 500 °C to 425 °C but also improved the yield of light olefin by 6.08%. The NH₃-TPD results illustrated that Fe-ZSM-5 has more strong acid sites than ZSM-5, the enhancement of strong acid sites is beneficial to the thermal cracking of LDPE, and the reduction in total acid sites helps to restrain the hydride transfer reactions of olefin, thus improving the yield of light olefin [22,25,50,51]. For olefin selectivity, it can be seen in Figure 8d that the content of C₂H₄ is lower than 1.70%, and the dominant gas components are C₃H₆ and C₄H₈.

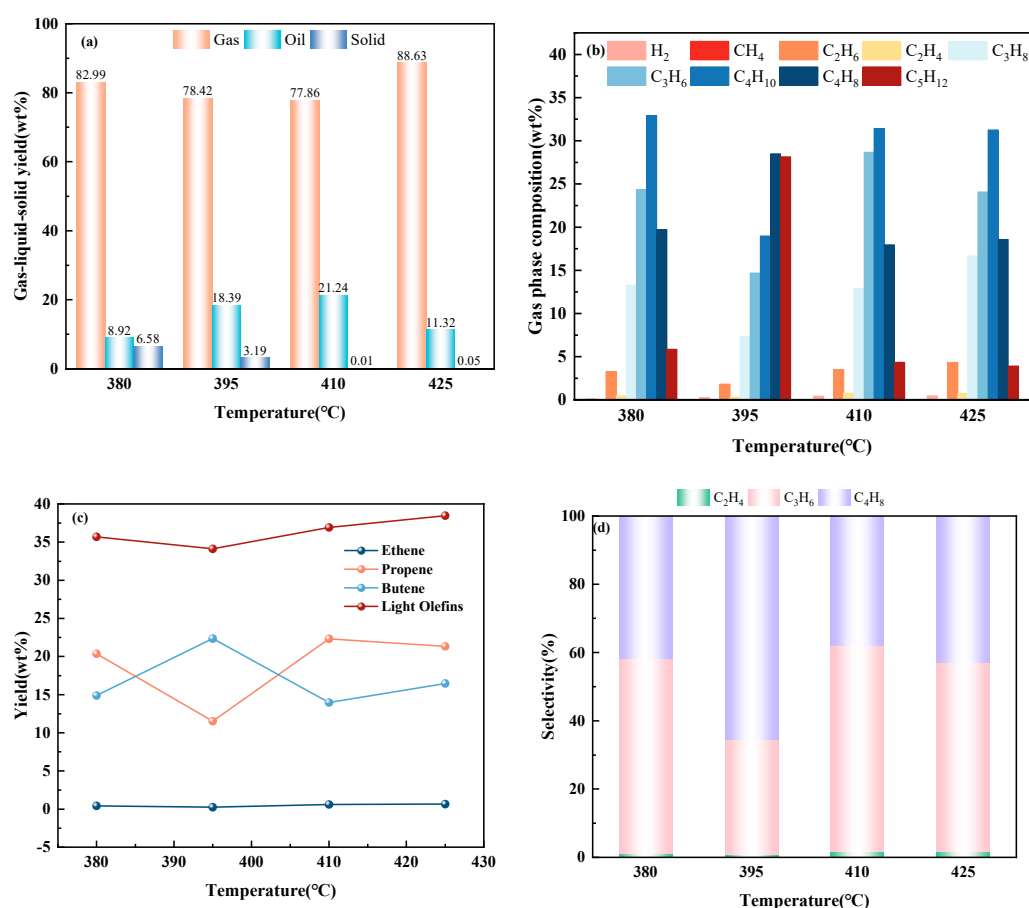


Figure 8. Influence of Fe-ZSM-5 on the creation of light olefin: (a) mass percentages of solids, gases, and liquids; (b) percentage by mass of H₂, CH₄, light olefin, and C₂–C₅ alkanes; (c) weight yields of light olefin; and (d) olefin selectivity of C₂H₄, C₃H₆, and C₄H₈.

2.2.4. Catalytic Performance of Fe-Mg-ZSM-5

Figure 9 shows the effects of Mg doping on the catalytic performance of Fe-ZSM-5. (Here, 1 wt% Mg is the optimal loading, and experimental data for different loadings of Mg is provided in the Supplementary Materials Figure S1.) It can be seen in Figure 9a that the gas yield on Fe-Mg-ZSM-5 at 395 °C reached 85.78 wt%, which is 7.36% higher than that of Fe-ZSM-5, and then increased slightly to 88.07% when the pyrolysis temperature further rose to 425 °C. The gas composition of LDPE catalytic pyrolysis on Fe-Mg-ZSM-5

(Figure 9b) is similar to that of the Fe-ZSM-5 and ZSM-5 catalysts, and the content of light olefin accounts for 45.31% of the total gas product at 395 °C. As displayed in Figure 9c, the highest light olefin yield of 38.87 wt% was obtained at 395 °C. It is evident that the Mg loading not only reduced the optimal pyrolysis temperature from 425 °C to 395 °C but also improved the yield of light olefin by 0.41 wt%. The NH₃-TPD results showed that the Mg loading decreased the strong acidity of Fe-ZSM-5, which can effectively improve the coking resistance and service life of the catalyst [43]. Fe-Mg-ZSM-5 also had a slight increase in medium acid sites compared with Fe-ZSM-5, which promotes the dehydrogenation cracking reaction and improves the selectivity of light olefins [52,53]. More importantly, it was found that the introduction of Mg significantly reduced the average particle size of Fe oxides on the catalyst from 40 nm to 10 nm, which is beneficial to improving the catalytic activity and thus decreasing the pyrolysis reaction temperature. Figure 9d shows that the major compounds in the gas product of LDPE catalytic pyrolysis on Fe-Mg-ZSM-5 are C₃H₆ and C₄H₈, which account for 53.93% and 44.43% at 395 °C, respectively.

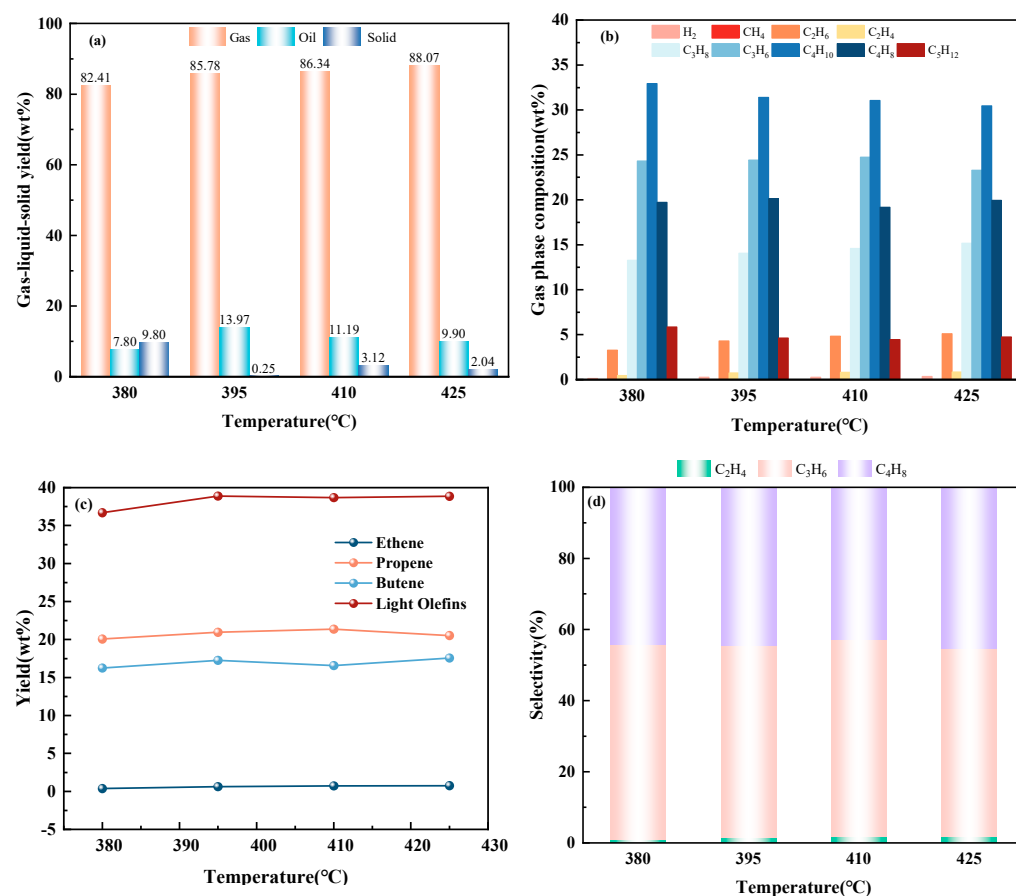


Figure 9. Influence of Mg loadings in Fe-ZSM-5 on the yields of light olefin: (a) mass percentages of solids, gases, and liquids; (b) percentage by mass of H₂, CH₄, light olefin, and C₂-C₅ alkanes; (c) weight yields of light olefin; and (d) olefin selectivity of C₂H₄, C₃H₆, and C₄H₈.

2.3. Analysis of Catalytic Performance

Based on the characterization results and catalytic pyrolysis performance of different catalysts, the probable catalytic performance is exhibited in Figure 10. It is believed that the degradation of LDPE takes place through a random chain cleavage mechanism of random chain break and end chain break [51,54], which mainly generates waxes and a wide range of hydrocarbons from C₁₂-C₂₁. Catalytic pyrolysis of LDPE on zeolites is guided by the carbonium ion theory [5,10,55], and the acidic sites play a key role in the catalytic cracking of LDPE [10,20].

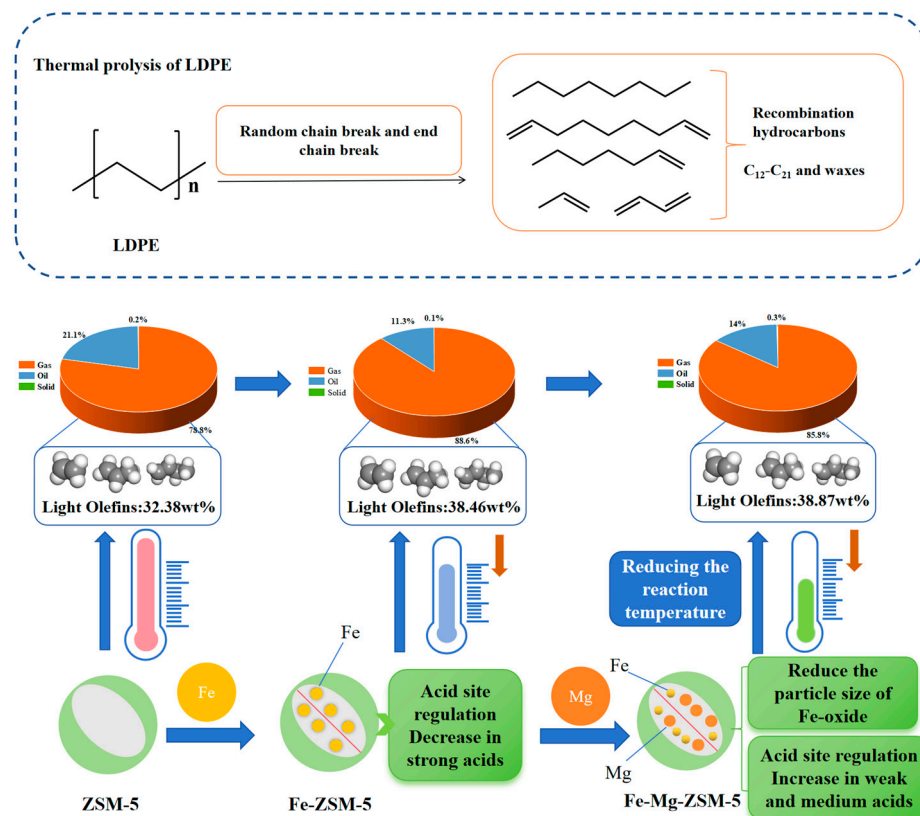


Figure 10. Catalytic pyrolysis performance of LDPE with different catalysts.

The NH_3 -TPD results showed that the loading of Fe oxides increased the strong acidity of ZSM-5. It is considered that the promotion of strong acidity is beneficial for the catalytic cracking of LDPE and leads to a decrease in the pyrolysis temperature. The loading of Mg on Fe-ZSM resulted in a decrease in strong as well as an increase in medium and weak acidity. Although the decrease in strong acidity has a negative effect on the catalytic pyrolysis of LDPE, it can inhibit the secondary crack and coking reactions of light olefin, which helps to prolong catalyst life. The increase in medium acidity promoted the transfer of hydrogen to short-chain alkanes and olefins [56]; subsequently, short-chain alkanes and olefins diffused into the pores of the zeolite and proceeded to the aromatization dehydrocyclization reaction. In addition, it can be seen from the SEM results that the average particle size of Fe oxides on Fe-Mg-ZSM-5 is much smaller than that of Fe-ZSM-5, which can effectively improve the catalytic activity of the sample and thus further reduce the pyrolysis reaction temperature.

2.4. Regeneration of Spent Catalysts

After the primary catalytic pyrolysis experiment, the spent catalyst was recovered and directly reused for the subsequent pyrolysis run. The obtained gas–liquid–solid three-phase yields are exhibited in Figure 11. These results show that the gas yield decreased significantly from 85.78% to 14.31% when Fe-Mg-ZSM-5 was reused for three cycles, indicating the catalyst is easily deactivated during the catalytic pyrolysis of LDPE. This is mainly associated with the formed coke deposited on the surface of the catalyst, resulting in the clogging of zeolite pores as well as the covering of acid sites [57].

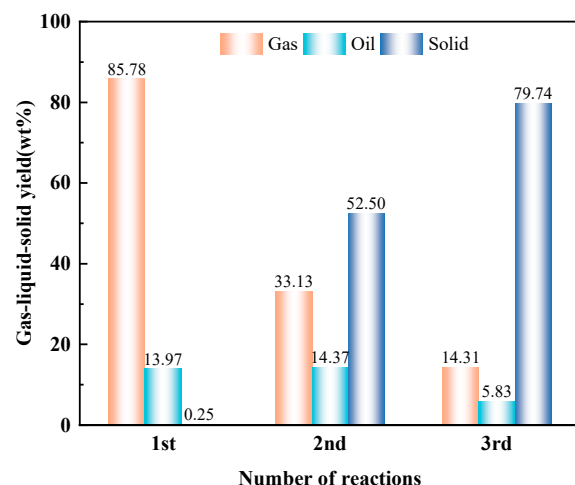


Figure 11. The catalytic performance of the spent Fe-Mg-ZSM-5 after being reused for three cycles.

In order to investigate the regeneration parameters of spent Fe-Mg-ZSM-5, a thermogravimetric analysis was performed in an air atmosphere with a heating rate of $10\text{ }^{\circ}\text{C}\cdot\text{min}^{-1}$. As illustrated in the TGA and DTG curves in Figure 12a, there are two major thermal degradation stages ranging from $30\text{ }^{\circ}\text{C}$ to $200\text{ }^{\circ}\text{C}$ and $200\text{ }^{\circ}\text{C}$ to $600\text{ }^{\circ}\text{C}$. The weight loss in the first stage is 4.02% , and an obvious endothermic peak centered at $186\text{ }^{\circ}\text{C}$ appears in the DTG curve, which is caused by the desorption of tar attached to the surface of the spent catalyst. The weight loss in the second stage is as high as 14.82% . The DTG curve shows that evident thermal degradation occurs in the temperature range of $400\text{ }^{\circ}\text{C}$ to $550\text{ }^{\circ}\text{C}$, with a maximum mass loss rate of about $425\text{ }^{\circ}\text{C}$; then, the weight remains unchanged when the temperature is higher than $550\text{ }^{\circ}\text{C}$, indicating the complete burning of the deposition coke on the spent catalyst. Therefore, we determined the regeneration parameters of the deactivated catalysts as follows: the spent catalysts were calcined at $600\text{ }^{\circ}\text{C}$ in airflow for 1 h with a heating rate of $10\text{ }^{\circ}\text{C}\cdot\text{min}^{-1}$.

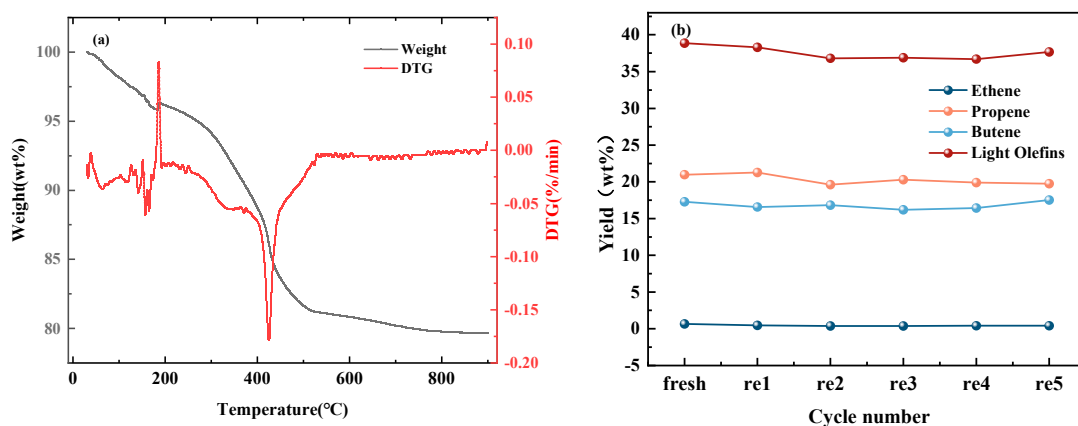


Figure 12. (a) TG and DTG curves of the spent Fe-Mg-ZSM-5. (b) The catalytic performance of the regenerated Fe-Mg-ZSM-5.

The regenerated catalysts were further reused for the catalytic pyrolysis of LDPE. It can be seen in Figure 12b that the regenerated Fe-Mg-ZSM-5 showed a similar catalytic performance as the fresh Fe-Mg-ZSM-5, indicating the prepared catalyst has an excellent regeneration property. After the first cycle, the light olefin yield decreased slightly from $38.87\text{ wt}\%$ to $38.30\text{ wt}\%$ and then remained stable even after five cycles. Furthermore, the yields of ethene, propene, and butene on the regenerated catalysts were almost as same as those on the fresh catalyst. The XRD diffraction of the deactivated and regenerated Fe-Mg-ZSM-5 samples is presented in Figure 13a. It can be seen that the regeneration

process has a negligible influence on the XRD spectrum of the spent Fe-Mg-ZSM-5 catalyst, suggesting the crystal structure of the Fe and Mg oxides remain unchanged during the high-temperature regeneration process.

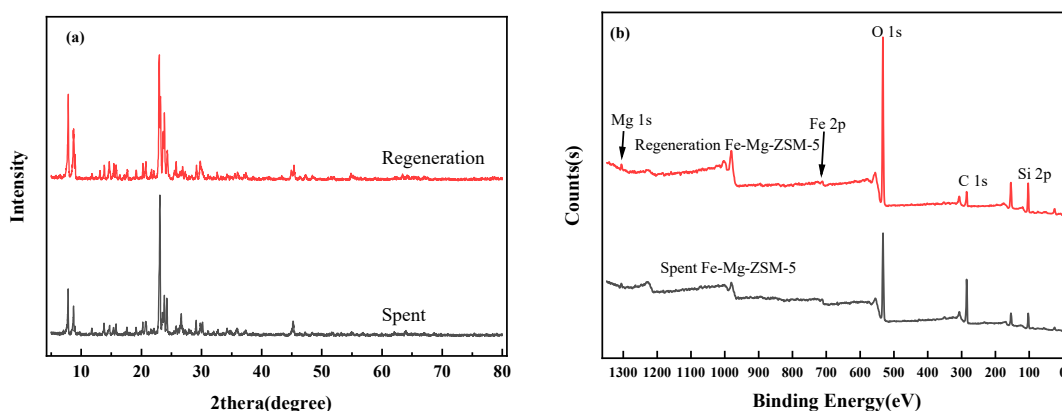


Figure 13. Characterization of the inactivated Fe-Mg-ZSM-5 and the regenerated Fe-Mg-ZSM-5: (a) XRD pattern and (b) XPS survey scan spectrum.

3. Materials and Methods

3.1. Sample Preparation

Powdered LDPE (100 mesh, Zhongyanshan Petrochemical Co., Ltd., Beijing, China) has been commercialized. The ZSM-5 zeolite used in this study was purchased from XFNANO company (Nanjing, China) with a ratio of SiO_2 -to- Al_2O_3 38 and a particle size of 530–580 μm . The Fe-ZSM-5 and Fe-Mg-ZSM-5 catalysts were prepared in the laboratory with incipient impregnation of ZSM-5 zeolite into aqueous solutions containing a metallic precursor of $\text{Fe}_2(\text{NO}_3)_3 \cdot 9\text{H}_2\text{O}$ and Mg $(\text{CH}_3\text{COO})_2 \cdot 4\text{H}_2\text{O}$ with different concentrations. In a typical operation, 15.0 g of ZSM-5 zeolites was impregnated in 10 mL of 0.26 mol/L $\text{Fe}_2(\text{NO}_3)_3 \cdot 9\text{H}_2\text{O}$ solution at room temperature, stirred for 2 h, and then dried at 110 $^\circ\text{C}$ for 3 h. The obtained sample was calcined at 550 $^\circ\text{C}$ in an air atmosphere for 5 h with a heating rate of 10 $^\circ\text{C}/\text{min}$, and the Fe-ZSM-5 catalyst with a 1 wt% Fe content was prepared. The synthesis method for the Fe-Mg-ZSM-5 catalysts with different Mg doping ratios was similar to that of the Fe-ZSM-5 catalyst except for the addition of different amounts of Mg $(\text{CH}_3\text{COO})_2 \cdot 4\text{H}_2\text{O}$ into the $\text{Fe}_2(\text{NO}_3)_3 \cdot 9\text{H}_2\text{O}$ solutions. The sample preparation flow chart is shown in Figure 14.

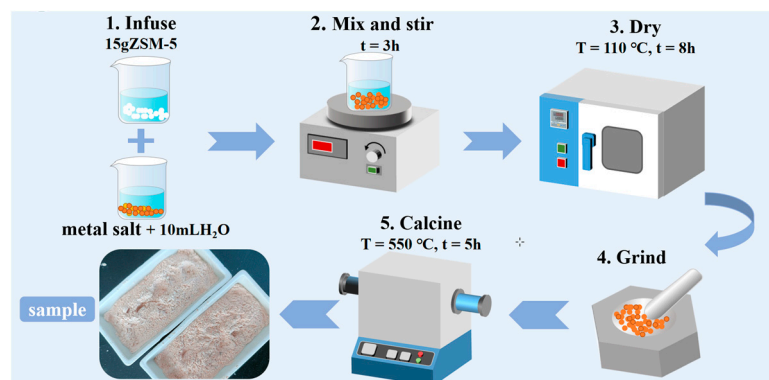


Figure 14. Preparation flow chart of the Fe-ZSM-5 and Fe-Mg-ZSM-5 samples.

3.2. Experimental Setup

All the pyrolysis experiments were performed in a N_2 atmosphere using a lab-scale fixed bed reactor, as shown in Figure S2. The device consisted of an electric heating tube furnace, a temperature-controlled system, a quartz reactor (ID = 50 mm, L = 440 mm), and a cooling system. In a typical run, 3 g of catalyst was mixed uniformly with 9 g of LDPE

sample (the mass proportion of the catalyst to LDPE was constant in all the experiments) and filled into the reactor. The tube furnace was firstly purged with 100 mL/min of N₂ for about 30 min and then was heated to the desired temperatures at a heating rate of 10 °C/min and held for 60 min.

The liquid products were gathered in glass bottles and cooled with an ice–water mixture, and then the gas phase products were collected in a bag. The weights of the liquid and solid products were determined directly using an analytical balance, and the qualities of the gas products were measured using the mass subtraction method, which was published by Carlson et al. [58]. The yield of gas, liquid, and solid products can be calculated with Formula (1), the yield of light olefin can be obtained with Formula (2), and light olefin selectivity can be measured with Formula (3).

$$\text{Yield of products (wt\%)} = \frac{\text{mass of solid, liquid, or gas products}}{\text{mass of feed}} \times 100\% \quad (1)$$

$$\text{Yield of light olefin (wt\%)} = \frac{\text{mass of C}_2 \text{ to C}_4 \text{ olefins}}{\text{mass of feed}} \times 100\% \quad (2)$$

$$\text{Light olefin selectivity (\%)} = \frac{\text{mass of an olefin product}}{\text{mass of all olefins}} \times 100 \quad (3)$$

In addition, all experiments were replicated 3 times to confirm the average errors of the results were less than 5%.

3.3. Characterization of the Samples

The physicochemical properties of the fresh, spent, and regenerated catalysts were characterized using X-ray diffraction (XRD), scanning electron microscopy (SEM), N₂ adsorption–desorption isotherms, programmed ramp-up desorption of ammonia (NH₃-TPD), X-ray diffraction photoelectron spectroscopy (XPS), high-resolution transmission electron microscopy (HRTEM), and thermogravimetric analysis (TGA). The details of the sample characterization method are given in the Supplementary Materials.

3.4. Product Analysis

The gas product collected in the gas bag was measured with GC-TCD (SP-6801AT). The main gas components detected with gas chromatography included H₂, CH₄, light olefins (C₂H₄, C₃H₆, and C₄H₈), C₂H₆, C₃H₈, and C₅H₁₂. The area normalization method was used to calculate gas composition and content. Detailed calculation methods can be found in the Supplementary Materials. Each gas sample was measured 3 times to obtain an average value.

4. Conclusions

Mg-modified Fe-ZSM-5 was used to catalyze the conversion of LDPE into light olefin for a lower pyrolysis temperature. The findings indicated that the types of catalysts, catalytic temperature, and Mg loading have an obvious influence on the generation of light olefin. The addition of Mg decreased the average particle size of Fe oxides, which could effectively reduce the pyrolysis temperatures. Meanwhile, the introduction of Mg into Fe-ZSM-5 inhibited the secondary reactions, thus improving the yields of light olefin. When the pyrolysis temperature was 395 °C and the Mg loading was 1 wt%, the highest yield of light olefin occurred at 38.87 wt%. The deactivation of catalysts can be easily regenerated with combustion in an air atmosphere. The yield of light olefin on the regenerated catalyst remained above 36.71 wt% after five cycles. In addition, a reasonable catalytic reaction path was proposed. This paper contributes to an in-depth understanding of the catalytic pyrolysis of LDPE to produce light olefin.

Supplementary Materials: The following supporting information can be downloaded at: <https://www.mdpi.com/article/10.3390/catal14010078/s1>, Figure S1: Influence of Fe-ZSM-5 with various Mg contents on the yields of light olefin: (a) mass percentages of solids, gases, and liquids; (b) mass percentages of H₂, CH₄, light olefin, and C₂–C₅ alkanes; (c) weight yields of light olefin; and (d) olefin selectivity of C₂H₄, C₃H₆, and C₄H₈; Figure S2: The pyrolysis experimental setup; Table S1: The physical properties of the catalysts; Table S2: The crystallinity of different samples.

Author Contributions: Conceptualization, Y.L.; methodology, Y.L.; validation, Y.L. and S.D.; investigation, X.L. and Q.M.; writing—original draft preparation, Y.L.; writing—review and editing, Y.L. and T.L.; supervision, X.W. and M.T.; project administration, H.Z. All authors have read and agreed to the published version of the manuscript.

Funding: This research was funded by the National Natural Science Foundation of China (22078168, NO. 52272086), the Taishan Scholar Project of Shandong Province (NO. tsqn202211178), and the Qingchuang Science and Technology Program of Shandong Province University (NO. 2019KJD004). Huawei Zhang, School of Environmental and Municipal Engineering, Qingdao University of Technology, Qingdao 266033, China.

Data Availability Statement: The data presented in this study are available in this article and the Supplementary Materials.

Acknowledgments: The authors are thankful to the anonymous reviewers for their useful suggestions.

Conflicts of Interest: The authors declare no conflicts of interest.

References

1. Lee, K.; Jing, Y.; Wang, Y.; Yan, N. A unified view on catalytic conversion of biomass and waste plastics. *Nat. Rev. Chem.* **2022**, *6*, 635–652. [[CrossRef](#)]
2. Ellis, L.D.; Rorrer, N.A.; Sullivan, K.P.; Otto, M.; McGeehan, J.E.; Román-Leshkov, Y.; Wierckx, N.; Beckham, G.T. Chemical and biological catalysis for plastics recycling and upcycling. *Nat. Catal.* **2021**, *4*, 539–556. [[CrossRef](#)]
3. Tao, L.; Ma, X.; Ye, L.; Jia, J.; Wang, L.; Ma, P.; Liu, J. Interactions of lignin and LDPE during catalytic co-pyrolysis: Thermal behavior and kinetics study by TG-FTIR. *J. Anal. Appl. Pyrolysis* **2021**, *158*, 105267. [[CrossRef](#)]
4. Danso, D.; Chow, J.; Streit, W.R. Plastics: Environmental and Biotechnological Perspectives on Microbial Degradation. *Appl. Environ. Microbiol.* **2019**, *85*, e01095-19. [[CrossRef](#)]
5. Peng, Y.; Wang, Y.; Ke, L.; Dai, L.; Wu, Q.; Cobb, K.; Zeng, Y.; Zou, R.; Liu, Y.; Ruan, R. A review on catalytic pyrolysis of plastic wastes to high-value products. *Energy Convers. Manag.* **2022**, *254*, 115243. [[CrossRef](#)]
6. Akgun, H.; Yapici, E.; Gunkaya, Z.; Ozkan, A.; Banar, M. Utilization of liquid product through pyrolysis of LDPE and C/LDPE as commercial wax. *Environ. Sci. Pollut. Res. Int.* **2021**, *28*, 45971–45984. [[CrossRef](#)] [[PubMed](#)]
7. Mohadjer Beromi, M.; Kennedy, C.R.; Younker, J.M.; Carpenter, A.E.; Mattler, S.J.; Throckmorton, J.A.; Chirik, P.J. Iron-catalysed synthesis and chemical recycling of telechelic 1,3-enchaind oligocyclobutanes. *Nat. Chem.* **2021**, *13*, 156–162. [[CrossRef](#)] [[PubMed](#)]
8. Aboul-Enein, A.A.; Awadallah, A.E. Production of nanostructured carbon materials using Fe–Mo/MgO catalysts via mild catalytic pyrolysis of polyethylene waste. *Chem. Eng. J.* **2018**, *354*, 802–816. [[CrossRef](#)]
9. Ding, K.; Liu, S.; Huang, Y.; Liu, S.; Zhou, N.; Peng, P.; Wang, Y.; Chen, P.; Ruan, R. Catalytic microwave-assisted pyrolysis of plastic waste over NiO and HY for gasoline-range hydrocarbons production. *Energy Convers. Manag.* **2019**, *196*, 1316–1325. [[CrossRef](#)]
10. Song, J.; Sima, J.; Pan, Y.; Lou, F.; Du, X.; Zhu, C.; Huang, Q. Dielectric Barrier Discharge Plasma Synergistic Catalytic Pyrolysis of Waste Polyethylene into Aromatics-Enriched Oil. *ACS Sustain. Chem. Eng.* **2021**, *9*, 11448–11457. [[CrossRef](#)]
11. Kumar, S.; Panda, A.K.; Singh, R.K. A review on tertiary recycling of high-density polyethylene to fuel. *Resour. Conserv. Recycl.* **2011**, *55*, 893–910. [[CrossRef](#)]
12. Zhang, S.; Yang, M.; Shao, J.; Yang, H.; Zeng, K.; Chen, Y.; Luo, J.; Agblevor, F.A.; Chen, H. The conversion of biomass to light olefins on Fe-modified ZSM-5 catalyst: Effect of pyrolysis parameters. *Sci. Total Environ.* **2018**, *628–629*, 350–357. [[CrossRef](#)] [[PubMed](#)]
13. Nawaz, Z. Light alkane dehydrogenation to light olefin technologies: A comprehensive review. *Rev. Chem. Eng.* **2015**, *31*, 413–436. [[CrossRef](#)]
14. Panda, A.K. Thermo-catalytic degradation of different plastics to drop in liquid fuel using calcium bentonite catalyst. *Int. J. Ind. Chem.* **2018**, *9*, 167–176. [[CrossRef](#)]
15. Anuar Sharuddin, S.D.; Abnisa, F.; Wan Daud WM, A.; Aroua, M.K. A review on pyrolysis of plastic wastes. *Energy Convers. Manag.* **2016**, *115*, 308–326. [[CrossRef](#)]
16. Yu, D.; Hui, H.; Li, S. Two-step catalytic co-pyrolysis of walnut shell and LDPE for aromatic-rich oil. *Energy Convers. Manag.* **2019**, *198*, 111816. [[CrossRef](#)]

17. Artetxe, M.; Lopez, G.; Elordi, G.; Amutio, M.; Bilbao, J.; Olazar, M. Production of Light Olefins from Polyethylene in a Two-Step Process: Pyrolysis in a Conical Spouted Bed and Downstream High-Temperature Thermal Cracking. *Ind. Eng. Chem. Res.* **2012**, *51*, 13915–13923. [[CrossRef](#)]
18. Nishu; Li, Y.; Liu, R. Catalytic pyrolysis of lignin over ZSM-5, alkali, and metal modified ZSM-5 at different temperatures to produce hydrocarbons. *J. Energy Inst.* **2022**, *101*, 111–121. [[CrossRef](#)]
19. Miandad, R.; Rehan, M.; Barakat, M.A.; Aburizaiza, A.S.; Khan, H.; Ismail IM, I.; Dhavamani, J.; Gardy, J.; Hassanpour, A.; Nizami, A.-S. Catalytic Pyrolysis of Plastic Waste: Moving Toward Pyrolysis Based Biorefineries. *Front. Energy Res.* **2019**, *7*, 27. [[CrossRef](#)]
20. Liu, T.; Li, Y.; Zhou, Y.; Deng, S.; Zhang, H. Efficient Pyrolysis of Low-Density Polyethylene for Regulatable Oil and Gas Products by ZSM-5, HY and MCM-41 Catalysts. *Catalysts* **2023**, *13*, 382. [[CrossRef](#)]
21. Li, Z.; Li, F.; Zhao, T.; Yu, H.; Ding, S.; He, W.; Song, C.; Zhang, Y.; Lin, H. The effect of steam on maximizing light olefin production by cracking of ethanol and oleic acid over mesoporous ZSM-5 catalysts. *Catal. Sci. Technol.* **2020**, *10*, 6618–6627. [[CrossRef](#)]
22. Wang, J.; Shan, J.; Tian, Y.; Zhu, T.; Duan, H.; He, X.; Qiao, C.; Liu, G. Catalytic cracking of n-heptane over Fe modified HZSM-5 nanosheet to produce light olefins. *Fuel* **2021**, *306*, 121725. [[CrossRef](#)]
23. Li, F.; Ding, S.; Wang, Z.; Li, Z.; Li, L.; Gao, C.; Zhong, Z.; Lin, H.; Chen, C. Production of Light Olefins from Catalytic Cracking Bio-oil Model Compounds over La₂O₃-Modified ZSM-5 Zeolite. *Energy Fuels* **2018**, *32*, 5910–5922. [[CrossRef](#)]
24. Lima, D.S.; Perez-Lopez, O.W. Catalytic conversion of glycerol to olefins over Fe, Mo, and Nb catalysts supported on zeolite ZSM-5. *Renew. Energy* **2019**, *136*, 828–836. [[CrossRef](#)]
25. Xia, S.; Zhu, Y.; Tian, Y.; He, X.; Guo, L.; Qiao, C.; Liu, G. Fe–Al isomorphous and self-pillared ZSM-5 nanosheet catalyst for cracking of n-heptane with enhanced selectivity of light olefins. *J. Energy Inst.* **2022**, *102*, 196–205. [[CrossRef](#)]
26. Shao, J.A.; Jiang, H.; Yang, M.; Xiao, J.; Yang, H.; Chen, Y.; Zhang, S.; Chen, H. Catalytic fast pyrolysis of cellulose over different metal-modified ZSM-5 zeolites for light olefins. *J. Anal. Appl. Pyrolysis* **2022**, *166*, 105628. [[CrossRef](#)]
27. Yang, M.; Shao, J.; Yang, Z.; Yang, H.; Wang, X.; Wu, Z.; Chen, H. Conversion of lignin into light olefins and aromatics over Fe/ZSM-5 catalytic fast pyrolysis: Significance of Fe contents and temperature. *J. Anal. Appl. Pyrolysis* **2019**, *137*, 259–265. [[CrossRef](#)]
28. Zheng, Y.; Wang, F.; Yang, X.; Huang, Y.; Liu, C.; Zheng, Z.; Gu, J. Study on aromatics production via the catalytic pyrolysis vapor upgrading of biomass using metal-loaded modified H-ZSM-5. *J. Anal. Appl. Pyrolysis* **2017**, *126*, 169–179. [[CrossRef](#)]
29. Schultz, E.L.; Mullen, C.A.; Boateng, A.A. Aromatic Hydrocarbon Production from Eucalyptus urophylla Pyrolysis over Several Metal-Modified ZSM-5 Catalysts. *Energy Technol.* **2017**, *5*, 196–204. [[CrossRef](#)]
30. Kostyniuk, A.; Key, D.; Mdleleni, M. Effect of Fe-Mo promoters on HZSM-5 zeolite catalyst for 1-hexene aromatization. *J. Saudi Chem. Soc.* **2019**, *23*, 612–626. [[CrossRef](#)]
31. Zhao, Y.; Liu, Q.; Cui, M.; Qiao, X.; Fei, Z. Mg/Ca modified hierarchical porous ZSM-5 zeolite for light-olefins production from chloromethane. *J. Porous Mater.* **2022**, *30*, 521–529. [[CrossRef](#)]
32. Abdalla, A.; Arudra, P.; Al-Khattaf, S.S. Catalytic cracking of 1-butene to propylene using modified H-ZSM-5 catalyst: A comparative study of surface modification and core-shell synthesis. *Appl. Catal. A Gen.* **2017**, *533*, 109–120. [[CrossRef](#)]
33. Gurdeep Singh, H.K.; Yusup, S.; Quitain, A.T.; Abdullah, B.; Ameen, M.; Sasaki, M.; Kida, T.; Cheah, K.W. Biogasoline production from linoleic acid via catalytic cracking over nickel and copper-doped ZSM-5 catalysts. *Environ. Res.* **2020**, *186*, 109616. [[CrossRef](#)] [[PubMed](#)]
34. Grandprix, T.M.; Kadja, T.R.S.; Ilimi, M.M.; Khalil, M.; Mukti, R.R. Subagjo Sequential mechanochemical and recrystallization methods for synthesizing hierarchically porous ZSM-5 zeolites. *Microporous Mesoporous Mater.* **2020**, *308*, 110550. [[CrossRef](#)]
35. Rahimi, S.; Rostamizadeh, M. Novel Fe/B-ZSM-5 nanocatalyst development for catalytic cracking of plastic to valuable products. *J. Taiwan Inst. Chem. Eng.* **2021**, *118*, 131–139. [[CrossRef](#)]
36. Chai, M.; Liu, R.; He, Y. Effects of SiO₂/Al₂O₃ ratio and Fe loading rate of Fe-modified ZSM-5 on selection of aromatics and kinetics of corn stalk catalytic pyrolysis. *Fuel Process. Technol.* **2020**, *206*, 106458. [[CrossRef](#)]
37. Kostyniuk, A.; Key, D.; Mdleleni, M. 1-hexene isomerization over bimetallic M-Mo-ZSM-5 (M: Fe, Co, Ni) zeolite catalysts: Effects of transition metals addition on the catalytic performance. *J. Energy Inst.* **2020**, *93*, 552–564. [[CrossRef](#)]
38. Yamashita, T.; Hayes, P. Analysis of XPS spectra of Fe²⁺ and Fe³⁺ ions in oxide materials. *Appl. Surf. Sci.* **2008**, *254*, 2441–2449. [[CrossRef](#)]
39. Li, M.; Liu, C.; Zhang, Z.; Cao, S.; Liu, H.; Shen, S.; Wang, W. Ultrathin Cu-Fe oxide nanosheets boosting persulfate activation to remove organic pollutants with coupling and transformation between radical and nonradical mechanism. *Sep. Purif. Technol.* **2022**, *281*, 119978. [[CrossRef](#)]
40. Ma, Y.; Zhang, D.; Sun, H.; Wu, J.; Liang, P.; Zhang, H. Fe–Ce Mixed Oxides Supported on Carbon Nanotubes for Simultaneous Removal of NO and Hg⁰ in Flue Gas. *Ind. Eng. Chem. Res.* **2018**, *57*, 3187–3194. [[CrossRef](#)]
41. Aksoy, S.; Caglar, Y.; Ilican, S.; Caglar, M. Sol-gel derived Li–Mg co-doped ZnO films: Preparation and characterization via XRD, XPS, FESEM. *J. Alloys Compd.* **2012**, *512*, 171–178. [[CrossRef](#)]
42. Lu, J.; Zhao, Z.; Xu, C.; Zhang, P.; Duan, A. FeHZSM-5 molecular sieves—Highly active catalysts for catalytic crackig of isobutane to produce ethylene and propylene. *Catal. Commun.* **2006**, *7*, 199–203. [[CrossRef](#)]

43. Ji, X.; Liu, B.; Ma, W.; Chen, G.; Yan, B.; Cheng, Z. Effect of MgO promoter on Ni-Mg/ZSM-5 catalysts for catalytic pyrolysis of lipid-extracted residue of *Tribonema minus*. *J. Anal. Appl. Pyrolysis* **2017**, *123*, 278–283. [[CrossRef](#)]
44. Wang, S.; Cao, B.; Liu, X.; Xu, L.; Hu, Y.; Afonaa-Mensah, S.; Abomohra, A.E.F.; He, Z.; Wang, Q.; Xu, S. A comparative study on the quality of bio-oil derived from green macroalga *Enteromorpha clathrata* over metal modified ZSM-5 catalysts. *Bioresour. Technol.* **2018**, *256*, 446–455. [[CrossRef](#)]
45. Ryu, H.W.; Lim, Y.H.; Jung, W.; Nam, K.; Hwang, Y.; Roh, J.E.; Kim, D.H. Enhanced stability of CO₂-assisted shale gas aromatization through the introduction of Mg promoter on Mo_ZSM-5. *Chem. Eng. J.* **2023**, *467*, 143404. [[CrossRef](#)]
46. Elordi, G.; Olazar, M.; Lopez, G.; Amutio, M.; Artetxe, M.; Aguado, R.; Bilbao, J. Catalytic pyrolysis of HDPE in continuous mode over zeolite catalysts in a conical spouted bed reactor. *J. Anal. Appl. Pyrolysis* **2009**, *85*, 345–351. [[CrossRef](#)]
47. Elordi, G.; Olazar, M.; Aguado, R.; Lopez, G.; Arabiourrutia, M.; Bilbao, J. Catalytic pyrolysis of high density polyethylene in a conical spouted bed reactor. *J. Anal. Appl. Pyrolysis* **2007**, *79*, 450–455. [[CrossRef](#)]
48. Aguado, J.; Serrano, D.P.; San Miguel, G.; Castro, M.C.; Madrid, S. Feedstock recycling of polyethylene in a two-step thermo-catalytic reaction system. *J. Anal. Appl. Pyrolysis* **2007**, *79*, 415–423. [[CrossRef](#)]
49. Wong, S.L.; Ngadi, N.; Abdullah TA, T.; Inuwa, I.M. Conversion of low density polyethylene (LDPE) over ZSM-5 zeolite to liquid fuel. *Fuel* **2017**, *192*, 71–82. [[CrossRef](#)]
50. Ji, Y.; Shi, B.; Yang, H.; Yan, W. Synthesis of isomorphous MFI nanosheet zeolites for supercritical catalytic cracking of n-dodecane. *Appl. Catal. A Gen.* **2017**, *533*, 90–98. [[CrossRef](#)]
51. Zhang, J.; Ma, M.; Chen, Z.; Zhang, X.; Yang, H.; Wang, X.; Feng, H.; Yu, J.; Gao, S. Production of monocyclic aromatics and light olefins through ex-situ catalytic pyrolysis of low-density polyethylene over Ga/P/ZSM-5 catalyst. *J. Energy Inst.* **2023**, *108*, 101235. [[CrossRef](#)]
52. Bai, Y.; Zhang, G.; Liu, D.; Zhang, Y.; Zhao, L.; Gao, J.; Xu, C.; Meng, Q.; Gao, X. The advance in catalytic pyrolysis of naphtha technology using ZSM-5 as catalyst. *Appl. Catal. A Gen.* **2021**, *628*, 118399. [[CrossRef](#)]
53. Ji, Y.; Yang, H.; Yan, W. Effect of alkali metal cations modification on the acid/basic properties and catalytic activity of ZSM-5 in cracking of supercritical n-dodecane. *Fuel* **2019**, *243*, 155–161. [[CrossRef](#)]
54. Inayat, A.; Inayat, A.; Schwieger, W.; Sokolova, B.; Lestinsky, P. Enhancing aromatics and olefins yields in thermo-catalytic pyrolysis of LDPE over zeolites: Role of staged catalysis and acid site density of HZSM-5. *Fuel* **2022**, *314*, 123071. [[CrossRef](#)]
55. Miandad, R.; Barakat, M.A.; Aburizaiza, A.S.; Rehan, M.; Nizami, A.S. Catalytic pyrolysis of plastic waste: A review. *Process Saf. Environ. Prot.* **2016**, *102*, 822–838. [[CrossRef](#)]
56. Bi, C.; Zhang, Z.; Han, D.; Wang, C.; Zhang, J.; Sun, M.; Hao, Q.; Chen, H.; Ma, X. Effective regulation of Ga active species in mesoporous ZSM-5 for catalytic upgrading of coal pyrolysis volatiles. *Fuel* **2022**, *321*, 124105. [[CrossRef](#)]
57. Lopez, A.; de Marco, I.; Caballero, B.M.; Adrados, A.; Laresgoiti, M.F. Deactivation and regeneration of ZSM-5 zeolite in catalytic pyrolysis of plastic wastes. *Waste Manag.* **2011**, *31*, 1852–1858. [[CrossRef](#)]
58. Carlson, T.R.; Cheng, Y.-T.; Jae, J.; Huber, G.W. Production of green aromatics and olefins by catalytic fast pyrolysis of wood sawdust. *Energy Environ. Sci.* **2011**, *4*, 145–161. [[CrossRef](#)]

Disclaimer/Publisher’s Note: The statements, opinions and data contained in all publications are solely those of the individual author(s) and contributor(s) and not of MDPI and/or the editor(s). MDPI and/or the editor(s) disclaim responsibility for any injury to people or property resulting from any ideas, methods, instructions or products referred to in the content.